energies

MDPI

Article

Numerical Investigation of Heat Transfer and Flow Dynamics in Tubes with DNA-Inspired Slotted Inserts

Penglong Zhu [1], Guoxiu Sun [2], Ruimeng Liu [1], Sicong Zhou [1], Baisong Hu [1,*] and Shaofeng Zhang [1]

[1] School of Chemical Engineering and Technology, Hebei University of Technology, Tianjin 300130, China; 202221502010@stu.hebut.edu.cn (P.Z.); 222001@stu.hebut.edu.cn (R.L.); 202331504012@stu.hebut.edu.cn (S.Z.); 1986037@hebut.edu.cn (S.Z.)

[2] Hebei Zetian Chemical Co., Ltd., Hengshui 053000, China; yf_20180101@sina.com

* Correspondence: hubaisong@hebut.edu.cn

Abstract: Within the realm of industrial energy conservation, the optimization of heat exchanger performance is paramount for the augmentation of energy utilization efficiency. This investigation employs computational fluid dynamics (CFD) simulations to elucidate the effects of an innovative DNA-Inspired Slotted Insert (DSI) on the convective heat transfer and pressure drop characteristics within heat exchange tubes. The study provides a thorough analysis of fully turbulent flow (Re = 6600–17,200), examining the effects of various DSI pitches, key lengths, and geometries. The findings reveal that the DSI instigates a three-dimensional spiral flow pattern, which is accompanied by an escalation in the Nusselt number (Nu) and friction factor (f) with increasing Reynolds numbers. An inverse relationship between Nu and both pitch and key length is observed; conversely, f exhibits a direct correlation with these parameters. The study identifies an optimal configuration characterized by a pitch of 10 mm and a key length of 1.5 mm, with square keys demonstrating superior heat transfer performance relative to other geometrical configurations. This research contributes significant design and application insights for double-helical inserts, which are pivotal for the enhancement of heat exchanger efficiency.

Keywords: numerical investigation; heat transfer enhancement; thermo-hydraulic performance



Academic Editor: Andrea Frazzica

Received: 9 December 2024
Revised: 27 December 2024
Accepted: 8 January 2025
Published: 16 January 2025

Citation: Zhu, P.; Sun, G.; Liu, R.; Zhou, S.; Hu, B.; Zhang, S. Numerical Investigation of Heat Transfer and Flow Dynamics in Tubes with DNA-Inspired Slotted Inserts. *Energies* **2025**, *18*, 376. https://doi.org/10.3390/en18020376

Copyright: © 2025 by the authors. Licensee MDPI, Basel, Switzerland. This article is an open access article distributed under the terms and conditions of the Creative Commons Attribution (CC BY) license (https://creativecommons.org/licenses/by/4.0/).

1. Introduction

With the dual objectives of improving energy utilization efficiency and achieving sustainable development, the development of new technologies aimed at enhancing the performance of heat exchangers and controlling energy consumption has become a focal point in the field of heat transfer. These advancements are primarily realized through two distinct technological approaches, aimed at improving the thermal efficiency of heat exchangers: active heat transfer enhancement and passive heat transfer enhancement techniques [1]. The present study primarily investigates the impact of internal inserts on the heat transfer performance of heat exchange tubes. The technology of adding internal inserts in tubes has garnered significant attention for its capability to markedly enhance turbulence, disrupt the boundary layer within the tube, and facilitate the heat transfer process. This technology not only increases the heat transfer efficiency, but also presents new possibilities for achieving economic and environmental sustainability with heat exchangers. The history of using internal inserts can be traced back to 1896; they are characterized by their simple fabrication, low cost, and ease of installation and disassembly. These advantages allow for a reduction in the size of heat exchange equipment under the same heat load, ultimately resulting in cost savings. Despite the significant benefits

associated with internal inserts, their application poses challenges, such as increased flow resistance, which potentially leads to higher pumping energy consumption. Additionally, the structural parameters of the inserts significantly impact the flow field, resistance, and heat transfer performance, making it imperative to study the optimal structural parameters through numerical simulation research [2–6].

Numerous studies have been conducted on internal inserts, which come in various forms, including twisted tapes, vortex generators, and helical springs, among others. Twisted tapes, a simple structure of internal inserts, are formed by twisting a flat strip along the axial direction at a certain angle. Varun's experimental and numerical investigations revealed that twisted tape inserts enhance heat transfer more effectively in laminar flow than in turbulent flow [7]. Yu et al. [8] further explored the impact of different twisted tape configurations on the heat transfer performance and flow resistance in helical tubes, demonstrating that the collaborative effect between hollow twisted tapes and helical tubes yielded the best overall performance. Vortex generators create rotational flow in the heat transfer process by inducing complex flow structures on the heat transfer surface, playing a pivotal role in enhancing heat transfer and lowering pressure drop [9]. An important parameter for evaluating heat transfer performance is the PEC (performance evaluation criterion), which has been extensively applied in the heat exchange domain due to its simplicity and clear physical significance [10]. Aliabadi et al. [11] developed a novel triangular-edge-finned insert which was found to significantly improve the heat transfer coefficient of the heat exchanger, with the combined performance index reaching 1.41, showcasing its potential for enhancing heat transfer efficiency.

Unlike twisted tapes, helical inserts are installed closer to the boundary layer region of the fluid, adjacent to the inner wall of the heat exchange tube. This design disrupts the development of the boundary layer as the fluid flows over the helical surface, increasing the convective heat transfer capability between the fluid in the boundary layer and the wall of the heat exchanger [12]. Helical springs not only enhance heat transfer, but also possess fouling resistance properties [12,13], adding tremendous value to the field of heat transfer [14]. Researchers have extensively studied the flow and heat transfer characteristics of helical inserts. Even et al. [15] demonstrated through experiments that inserting inclined helical springs in the tube significantly influences heat transfer and friction loss, with the spring angle having a more substantial effect than the quantity of springs. Gunes et al. [16] investigated the heat transfer and pressure drop in tube bundles with helical inserts, revealing that the Nusselt number increases with Reynolds number and wire thickness, while it decreases with spacing. Omidi et al. [17] performed a numerical analysis of helical parabolic heat exchangers, finding that the temperature difference decreased significantly across the insert as the number of blades increased, resulting in a more uniform temperature distribution due to vortex flow. Dbouk et al. [18] conducted numerical simulations comparing straight, helical, and chaotic tubes, demonstrating that the chaotic tube outperformed the others. Mansour et al. [19] analyzed the thermal performance of seven different helical geometries, finding that higher coil spacing is required for enhancing heat transfer at lower Reynolds numbers. Zhang et al. [20] examined heat transfer and friction loss characteristics in flat tubes with double-helical springs, observing that the fluid exhibited a three-dimensional spiral flow, with both circumferential and radial velocities increasing near the wall. Through diverse structural designs, helical inserts have effectively enhanced the heat transfer efficiency of heat exchangers while controlling increases in energy consumption. The developments in these technologies provide new insights for the design and optimization of heat exchangers, which is crucial for achieving efficient energy utilization and environmental sustainability.

Helical structures and vortex generators are also common internal flow disruptors. The helical structure, resembling a conical frustum, is an annular-shaped internal flow disruption element that is widely used in heat exchangers for heat transfer enhancement, due to its simple structure, low cost, and efficacy in heat transfer augmentation. Vipin et al.'s [21] research highlights the potential of conical orificed rings for increasing the Nusselt number, while Nakhchi and Esfahani's [22] study provides an optimized design for a perforated hollow cylindrical insert to achieve higher heat transfer efficiency and lower flow resistance. Vortex generators refer to specific structures that are regularly arranged on the heat transfer surface during convective heat transfer processes, inducing an axis-rotating motion in the fluid, thereby generating vortices. These special structures alter the distribution and flow conditions of the fluid's secondary flow, reduce the boundary layer thickness, and enhance the intensity of turbulence, playing a significant role in improving heat transfer performance and reducing pressure drop. Consequently, they hold substantial value in the field of heat transfer [23–25]. In addition to common internal inserts, bio-inspired structures based on the surface morphology of biological organisms, such as fish fin protrusions, leaf vein fractals, and insect cuticular structures, have been widely applied in the development of enhanced heat exchange surfaces [26,27].

These structures leverage efficient natural heat transfer mechanisms to significantly improve heat transfer efficiency. Milad et al. [28] introduced DNA-inspired helical coil inserts, including double wire coils (DWCs) and triple wire coils (TWCs), to enhance the thermo-hydraulic performance of standard tubes. Under fully turbulent conditions, their proposed inserts significantly improved heat transfer performance and PEC values, while increasing the number of coils to three or more did not significantly enhance the PEC value. Andrew [29] utilized DNA-shaped inserts to significantly improve the heat transfer efficiency of heat exchangers, indicating their promising potential for future research in thermodynamics. The application of bio-inspired structures at micro-scales demonstrates their potential in enhancing heat transfer and reducing resistance. With a deeper understanding of the mechanisms behind bio-inspired designs and advancements in optimization methods, these structures are poised to play a more significant role in future heat transfer technologies.

Although the application of biomimetic structures on a macro scale has become quite prevalent, their utilization in environments that are constrained in terms of volume and mass is still in its infancy. In this study, we harness the structural principles of DNA and the velocity distribution characteristics of fluids within tubes to engineer an innovative double-helix coil insert known as the DNA-Inspired Slotted Insert (DSI). This design is intended to optimize heat transfer performance while managing excessive resistance. The research objective is to conduct numerical simulations to assess the influence of the DSI's structural parameters on heat transfer efficiency, and to determine the optimal configuration that maximizes energy utilization. The findings will offer valuable insights for the development and application of future internal inserts.

2. Materials and Methods

With the advancement of computational fluid dynamics (CFD), the numerical simulation of fluid mechanics problems has been significantly enhanced, overcoming the limitations of traditional experimental methods. Fluent, as a mainstream software in CFD, simulates fluid motion, heat transfer, and mass transfer by discretizing mathematical equations, providing insights into flow, temperature, and pressure distributions. For complex internal inserts, even slight geometric variations can lead to significant performance changes, emphasizing the importance of conducting numerical simulations under

consistent boundary conditions. In summary, Fluent plays an indispensable role in fluid mechanics research, due to its robust simulation capabilities.

2.1. Physical Model

The design of the DSI involves truncating the keys within a double-helical structure to create short keys. This design not only enhances heat transfer efficiency, but effectively controls energy loss due to increased fluid resistance. Through this innovative structural adjustment, the DSI enhances heat transfer performance while maintaining hydraulic efficacy, providing a new solution for the design of heat exchangers. A schematic diagram of the DSI is available in Figure 1a,b, along with the structural parameters detailed in Figure 1c. The fluid under investigation is water; the heat exchange tube is constructed of steel, with an internal diameter of 22 mm and an inlet temperature of 290 K, and the outer surface of the heat exchange tube is an isothermal wall with a temperature Tw = 353 K. Consequently, a static pressure outlet (the outlet pressure is equal to zero) is used as the outlet condition. The diameter of the internal insert D = 21 mm, the wire diameter e = 2 mm, and key diameter s = 1 mm. The specific research conditions are detailed in Table 1.

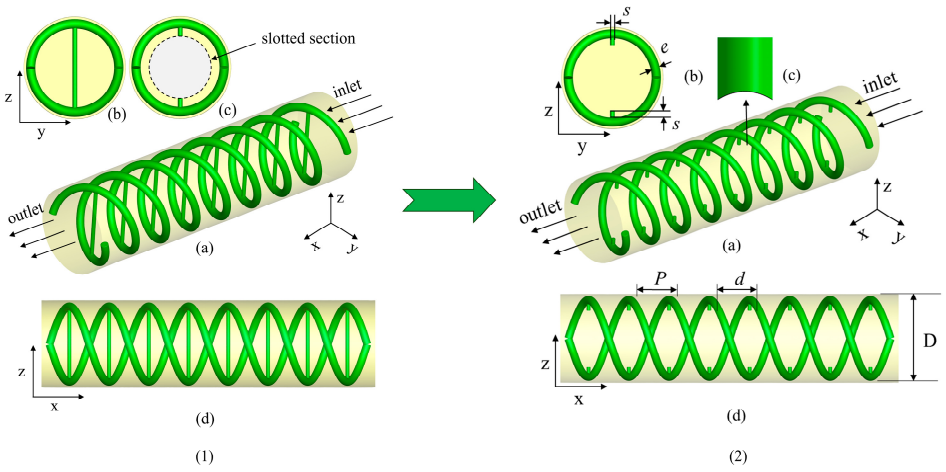


Figure 1. Schematic diagram of DSI: (**a**) 3D view of tube with DSI; (**b**) y–z view; (**c**) schematic diagram of slotted section; (**d**) x–z view.

Table 1. Research conditions.

Geometric Parameter	p (mm)	d_0 (mm)	Key Shape
Case 1	10	1	Circular
Case 2	15	1.5	Equilateral
Case 3	20	2	Triangular

2.2. Numerical Model

2.2.1. Governing Equations and Boundary Conditions

To establish the mathematical model, the following simplifying assumptions were made for the CFD model:

1. The flow is assumed to be steady and fully developed turbulent (periodic boundary conditions facilitate repeated flow solutions);
2. The physical properties of the fluid and the internal insert are considered constant;
3. The wall thickness of the tube is considered negligible;
4. Heat radiation and natural convection are ignored (considered perfectly insulated tubes);
5. Gravity and inlet effects are neglected.

Continuity equation:

$$\frac{\partial(\rho u_i)}{\partial x_i} = 0 \tag{1}$$

Momentum equation:

$$\frac{\partial}{\partial x_i}(\rho u_i u_k) = \frac{\partial}{\partial x_i}\left(\mu \frac{\partial u_k}{\partial x_i}\right) + \frac{\partial_p}{\partial x_k}(k = 1, 2, 3) \tag{2}$$

Energy equation for the fluid phase:

$$\frac{\partial}{\partial x_i}(\rho c_p u_i T) = \frac{\partial}{\partial x_i}\left(\lambda f \frac{\partial T}{\partial x_i}\right) \tag{3}$$

Energy equation for the solid phase:

$$\frac{\partial}{\partial x_i}\left(\lambda s \frac{\partial T}{\partial x_i}\right) = 0 \tag{4}$$

2.2.2. Computation Scheme

In the numerical simulation, we employed the Realizable k-ε turbulence model coupled with enhanced wall treatment, which is known for its superior performance in handling complex boundary layer flows characterized by rotation, separation, strong adverse pressure gradients, and recirculation. The pressure–velocity coupling was addressed using the SIMPLE algorithm, while the discretization of the momentum and energy equations was carried out with second-order accuracy for both pressure and up-wind schemes. The simulation was considered converged when the continuity equation reached a convergence criterion of 10^{-6}, the momentum equation achieved the same level, and the energy equation settled at 10^{-8}. Iterations were continued until the parameters of pressure gradient, outlet temperature, and outlet velocity exhibited negligible changes, indicating that the solution had stabilized according to the predefined convergence criteria. Notably, the surface for calculating the Nusselt number (Nu) was identified as the fluid–solid coupling surface of the heat exchange tube.

2.3. Data Reduction

The following equations were utilized to analyze the numerical results:

Reynolds number (*Re*):

$$Re = \frac{Du\rho}{\mu} \tag{5}$$

where D is the internal diameter of the heat exchange tube, u is the fluid velocity, ρ is the fluid density, and μ is the fluid's viscosity.

Friction factor (f):

$$f = \frac{p}{\frac{1}{2}\rho u_m^2 \frac{L}{D}} \tag{6}$$

where q is the pressure drop in the heat exchange tube, u_m is the average fluid velocity, and L is the length of the heat exchange tube.

Heat transfer coefficient (h):

$$h = \frac{q}{T_w - T_f} \tag{7}$$

where q is the wall heat flux, T_w is the temperature of the wall surface, and T_f is the bulk fluid temperature.

Nusselt number (Nu):

$$Nu = \frac{hD}{\lambda} \tag{8}$$

where λ is the thermal conductivity of the fluid.

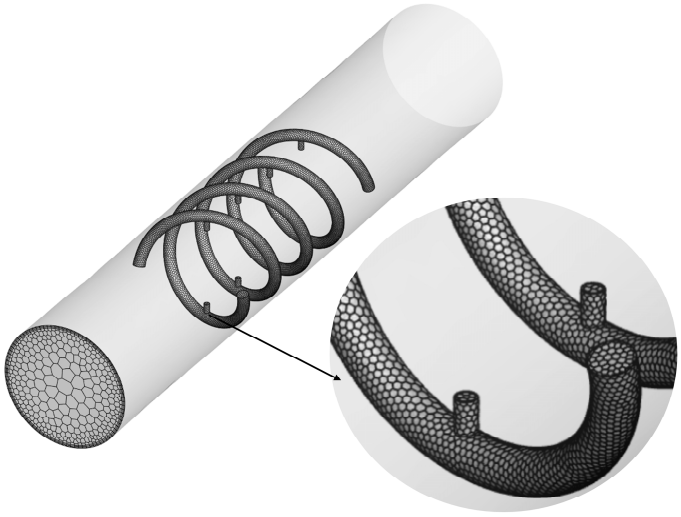
Performance evaluation coefficient (*PEC*):

$$PEC = \frac{\frac{Nu_i}{Nu_0}}{\left(\frac{f_i}{f_0}\right)^{\frac{1}{3}}} \quad (9)$$

where Nu_i and Nu_0 denote the Nusselt numbers of the enhanced and smooth tubes, respectively, and f_i and f_0 denote the friction factors of the enhanced and smooth tubes, respectively. A PEC value of less than 1 indicates insufficient enhanced convective heat transfer to justify the negative effects of increased pumping power.

2.4. Grid Dependency

The verification of grid independence is an essential step in computational fluid dynamics simulations. By progressively refining the grid and comparing simulation results across different grid densities, the stability of the results is established, ensuring that simulation accuracy is not affected by grid density. Rectangular elements were used for meshing the wall and surface of the insert; tetrahedral meshes were applied to the internal volume of the heat exchange tube, as illustrated in Figure 2. Furthermore, local grid refinement was adopted in the boundary layer region to enhance calculation precision. To ensure that the boundary layer is well-resolved, the Y+ value, a dimensionless quantity used to characterize the distance of the grid from the wall in wall-bounded turbulent flows, should be within the range of 5 < Y+ < 30.This range is considered optimal for capturing the near-wall turbulence characteristics accurately. To validate grid independence and test the numerical results against the mesh density, grid-related tests are indispensable. Four different meshes were generated for calculating the friction factors and Nusselt numbers at maximum velocity and Reynolds number, as shown in Table 1. It should be noted that a grid system with 7,540,000 cells was employed for subsequent calculations, since the variations in the parameters were less than 1%, even with further grid refinements.



(1)

Grid number	6,625，533	7,540,678	8,340,916	10,340,639
Nu	194	193	193	193
f	0.154	0.154	0.154	0.154

(2)

Figure 2. Grid dependency. (**1**) Boundary mesh at inlet and inserted tape surface. (**2**) Grid number.

2.5. Comparison of Simulation Data with Experimental Data

The numerical results for the smooth tube were compared with the empirical formula proposed by Gnielinski [4] and for the DSS [30] (Double Spiral Spring), and the simulation results were compared with the experimental data from Jafari, as shown in Figure 3. The comparison demonstrated minimal discrepancies between the simulation and experimental results, with the maximum error not exceeding 5.14% and the minimum error not falling lower than 3.56%, and relative errors maintained within ±6%. This confirms the applicability of the computational model utilized in this simulation.

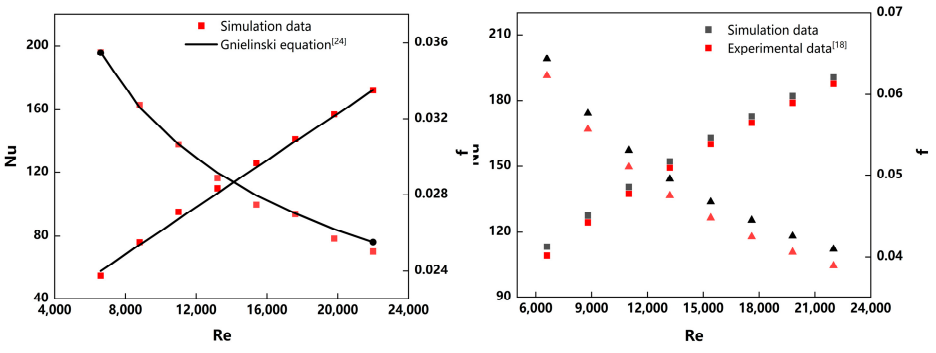


Figure 3. The comparison of the numerical results with the experimental results. (**a**) The comparison of the smooth tube. (**b**) The comparison of the DSS tube.

3. Results and Discussion

3.1. DSI Characteristics Study

3.1.1. Flow Characteristics

Figure 4 illustrates a comparative analysis of the velocity distributions at x = 755 mm for the smooth tubes, tubes with DSS, and tubes with DSI at a Reynolds number of 11,000. The analysis revealed that the presence of the insert in the tube significantly alters its velocity distribution compared to the smooth tube. Specifically, the velocity variation in the x-direction for the DSI tube is not significantly different from that of the DSS tube; however, notable changes are observed in the y-direction and z-direction velocities. This phenomenon indicates that the existence of keys within the DSI facilitates secondary flow in the tube, enhancing swirling effects and generating higher shear and radial velocities near the inner wall. The swirling effect accelerates the mixing between the main flow region and the near-wall region, thereby improving the tube's heat exchange and flow characteristics.

3.1.2. Vector Field Characteristics

As shown in Figure 5, a comparative analysis of the fluid dynamic characteristics of traditional smooth pipes, DSS pipes, and DSI pipes was conducted using vector field visualization techniques. It was observed that the DSS pipe enhances fluid mixing and heat transfer efficiency through helical flow, while the DSI pipe introduces vortices through structural keys, further increasing the turbulence of the fluid. The vector field images clearly illustrate the helical flow pattern within the DSS pipe and the complexity of fluid flow within the DSI pipe, particularly the changes in fluid direction and velocity near the key structures, thereby significantly enhancing the fluid dynamic performance of both types of pipes.

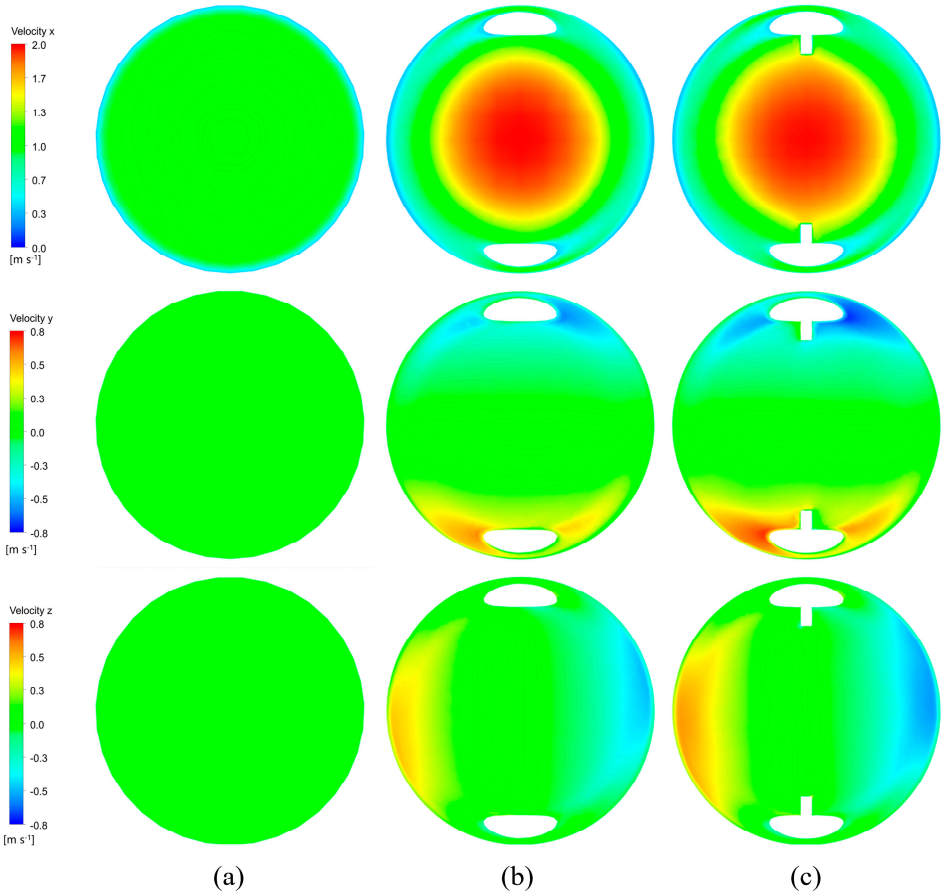


Figure 4. Velocity contour diagram of x = 755 mm longitudinal section. (**a**) Plain tube. (**b**) Tube with DSI inserted. (**c**) Tube with DSS inserted.

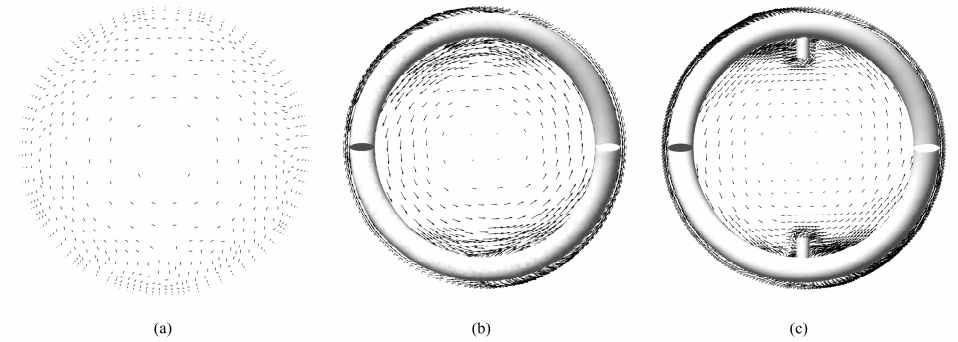


Figure 5. Vector field diagram of x–y plane longitudinal section. (**a**) Plain tube. (**b**) Tube with DSS inserted. (**c**) Tube with DSI inserted.

3.1.3. Pressure Characteristics

Figure 6 presents a comparative analysis of the pressure distribution along the x–y plane for smooth tubes, tubes with DSS, and tubes with DSI at a Reynolds number of 11,000. The results indicate that the presence of the internal insert significantly increases the pressure loss in the heat exchanger. Specifically, the introduction of the insert lengthens the flow path and increases flow complexity, requiring the fluid to overcome greater frictional resistance during its passage through the heat exchanger, resulting in elevated pressure drops. Quantitatively, the pressure drops in the tubes with the DSI and DSS are 7.47 times and 8.28 times higher than that of the smooth tube, respectively. The research finds that while internal inserts can enhance fluid thermal exchange efficiency, they also contribute to considerable pressure losses. Consequently, it is essential to consider both thermal exchange

efficiency and fluid resistance when designing heat exchangers, in order to achieve optimal performance balance.

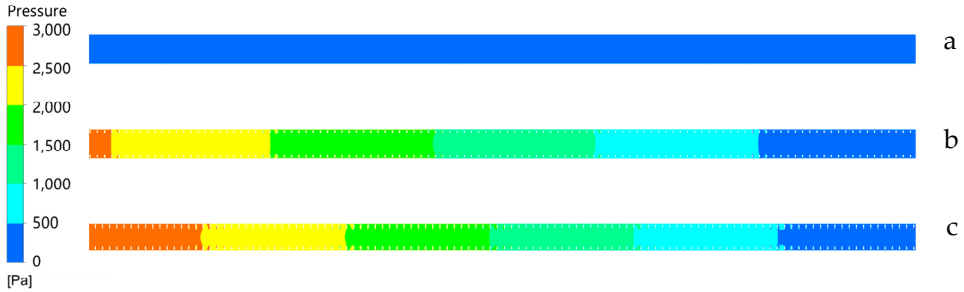


Figure 6. Pressure diagram of x–y plane longitudinal section. (**a**) Plain tube. (**b**) Tube with DSS inserted. (**c**) Tube with DSI inserted.

3.1.4. Turbulence Kinetic Energy Characteristics

In Figure 7, the turbulence kinetic energy contours at x = 755 mm for both the DSI and DSS tubes (with Re = 11,000) are analyzed in detail. In Figure 7a–c, the distribution of turbulent kinetic energy is depicted for three distinct cases: the smooth pipe, the DSS tubes, and the DSI tubes, respectively. The results indicate that both the DSI and DSS tubes exhibit significantly increased turbulence kinetic energy compared to the smooth tube, demonstrating the effective enhancement of turbulence with the use of internal inserts. The primary reason for this increase is attributed to the presence of keys in the DSI structure. The keys alter the flow path and velocity distribution of the fluid, promoting the formation of spiral flow and increasing the mixing and momentum exchange, thereby enhancing the heat transfer efficiency and improving the fluid dynamic characteristics.

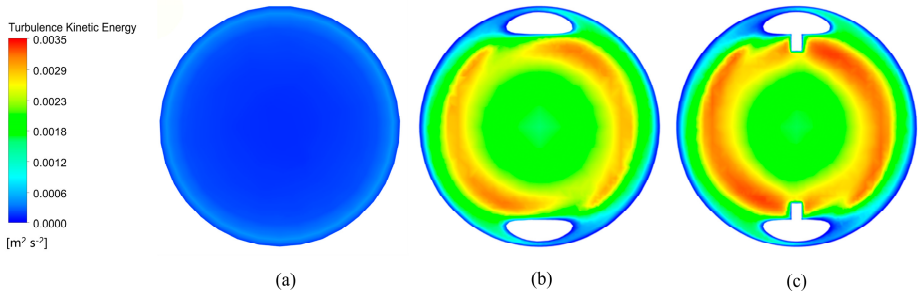


Figure 7. Turbulence kinetic energy diagram of x = 755 mm longitudinal section. (**a**) Plain tube. (**b**) Tube with DSS inserted. (**c**) Tube with DSI inserted.

3.1.5. Temperature Characteristics

Figure 8 illustrates the temperature distribution differences among the smooth tube, the tube with DSS, and the tube with DSI. The temperature distribution in the smooth tube is relatively uniform, with smooth axial changes. In contrast, the tubes with inserts exhibit shorter low-temperature regions, indicating that the fluid experiences a more rapid temperature increase in these sections. The presence of the insert promotes heat exchange within the fluid, especially in regions of intense turbulence, resulting in more effective thermal interaction between the fluid and the tube wall. The DSI tube demonstrates superior heat transfer performance at all four investigated locations compared to the DSS tube. Furthermore, k-m illustrate the temperature distribution in the heat exchange tubes with DSI over half a pitch, displaying a periodic helical variation in high-temperature regions that confirms the positive heat transfer effects initiated by the DSI.

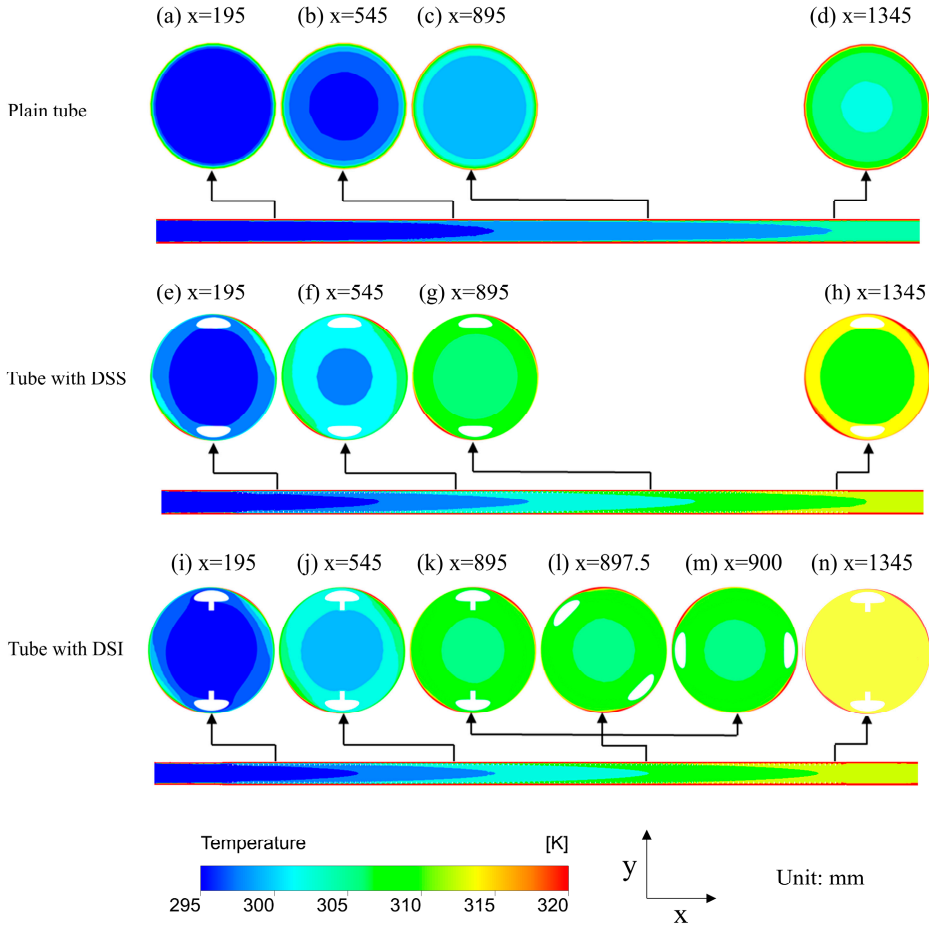


Figure 8. Temperature field comparison between the research object and the smooth tube at different locations.

3.2. Impact of DSI Structural Parameters

The pitch, key length and key shape of the internal insert influence the flow state and heat transfer performance within the heat exchange tube. This section discusses the impact of internal insert structural parameters on heat transfer capabilities and identifies the optimal DSI parameters based on performance evaluation.

3.2.1. Effect of Pitch

Under constant wall temperature conditions, Figure 9 presents the temperature distribution contours at z = 0 mm for DSI heat exchange tubes with three different pitches at Re = 11,000. The analysis indicates that with an increase in pitch, the low-temperature region within the heat exchange tube enlarges, while the outlet temperature exhibits a decreasing trend. This phenomenon can be explained by the fact that an increase in pitch results in a larger spacing between adjacent turns, thereby diminishing disruption and guidance effects on the fluid; moreover, an increased pitch also reduces the effective heat exchange area. These two factors collectively lead to a decrease in overall heat exchange, affecting the outlet temperature.

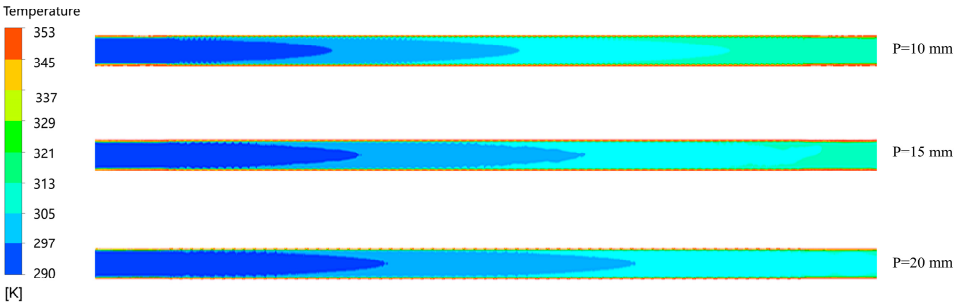


Figure 9. Temperature diagram of z = 0 mm longitudinal section.

Figure 10 summarizes the variations in the Nusselt number, friction factor, and PEC as a function of the Reynolds number under different pitches. It can be observed that at a fixed pitch, the Nusselt number gradually increases with an increase in the Reynolds number, while the friction factor and PEC show a downward trend. This phenomenon can be attributed to the intensifying turbulence within the fluid at higher Reynolds numbers, which enhances the thermal interactions between the fluid and solid surfaces. The internal vortices and irregular flow effectively remove heat from the surface, raising the Nusselt number. Simultaneously, turbulent motion decreases the velocity gradients between the fluid and the tube wall, lowering the viscous friction and resulting in a reduced friction factor. As PEC considers both heat transfer efficiency and pressure drop losses, despite the heat transfer efficiency improving at higher Reynolds numbers, the increasing pressure drop results in a declining PEC value.

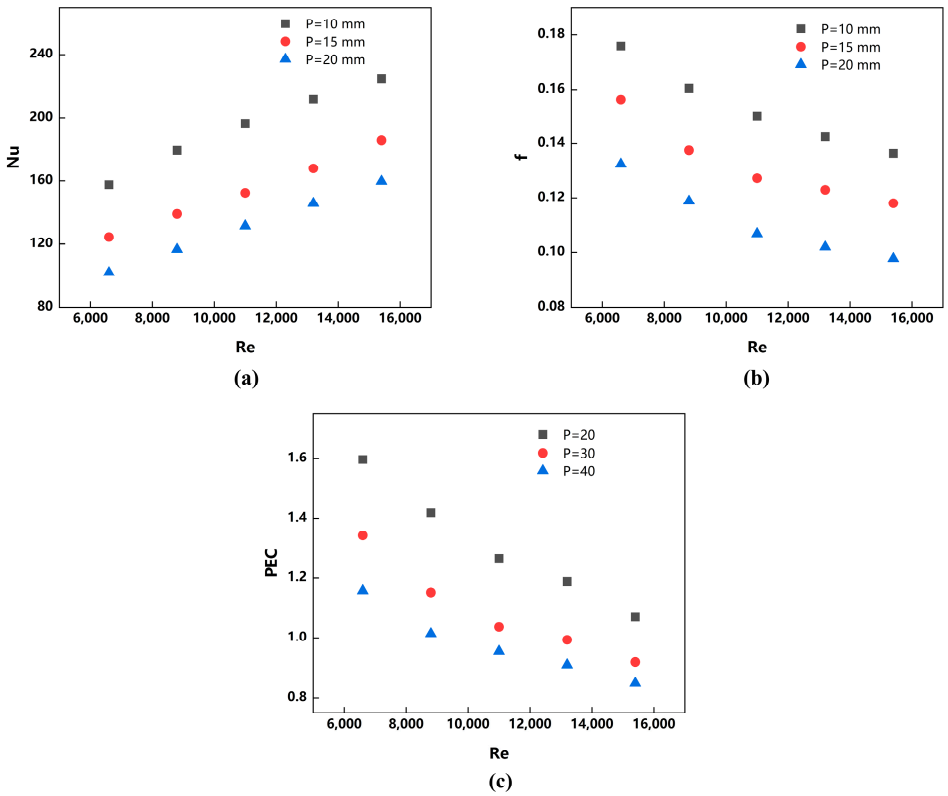


Figure 10. Variation in (**a**) Nusselt number, (**b**) friction factor, and (**c**) PEC, in terms of various pitches.

Additionally, it is evident from the figure that as the pitch increases, both the Nusselt number and the friction factor also increase. The DSI with a pitch of 10 mm yields the highest PEC, and its value exceeds 1, indicating a superior heat transfer performance relative to pumping power loss. In contrast, the DSI with a pitch of 20 mm has the lowest

PEC. This trend can be attributed to the increased pitch reducing the frequency of fluid disturbances per unit length of the helical insert, weakening the local turbulence and vortex formation between the fluid and the insert, thus reducing the additional frictional resistance and lowering the Nusselt number. The DSI with P = 10 mm outperforms those with P = 15 mm and P = 20 mm by 21.1%~26.6% and 40.8%~55.4% in Nusselt numbers, respectively. Moreover, the friction factor (f) for the DSI with P = 10 mm increases by 12.7%~15.7% and 32.7%~39.7% compared to the other two pitches. This indicates that pitch significantly influences heat exchange performance, and judicious selection of pitch is important for optimizing thermal performance and minimizing energy losses.

3.2.2. Effect of Key Length

To thoroughly investigate the impact of DSI key length on the overall performance of the heat exchanger, this study analyzed the equivalent diameter of the low-temperature region at x = 755 mm under four distinct operational conditions. These conditions correspond to four different DSI key lengths, namely 2 mm, 1.5 mm, 1 mm, and 0 mm. The four subfigures (a) through (d) in the figure respectively display the temperature distribution maps corresponding to these key lengths, with the diameters of the low-temperature regions being denoted as L1, L2, L3, and L4. The four subfigures (a) to (d) in the figure below each represent one of these key lengths. The gradual increase in the diameter of the low-temperature region as the DSI key length decreases indicates that a shorter key length enhances the heat transfer within the fluid in the heat exchange tube, effectively elevating the average temperature across the cross-section. This observation highlights the role of DSI key length in augmenting thermal performance within the heat exchanger system. The corresponding values of Nusselt number, friction factor (f), and PEC are illustrated in Figure 11.

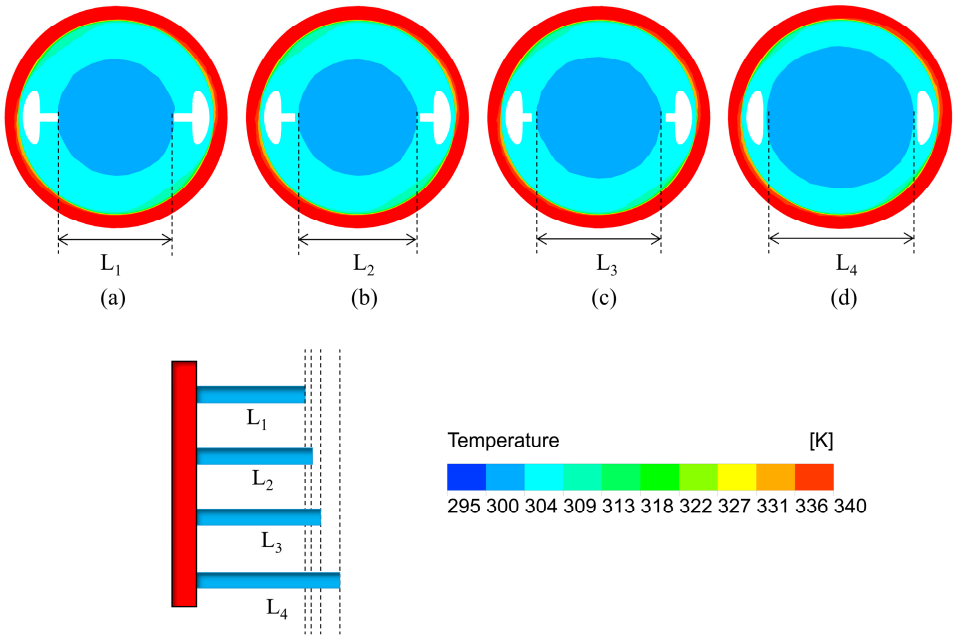


Figure 11. Temperature diagram of x = 755 mm longitudinal section (**a**) d_0 = 2 mm; (**b**) d_0 = 1.5 mm; (**c**) d_0 = 1 mm; (**d**) d_0 = 0 mm.

As depicted in Figure 12, the Nusselt numbers of both the DSI tubes and the DSS tubes increase with the Reynolds number for a given key length. Concurrently, the friction factor decreases as the PEC gradually declines. It can also be observed that a longer key length corresponds to higher Nusselt numbers and friction factors. Within the examined range of Reynolds numbers, the DSI tubes demonstrated a 3% to 7% enhancement in Nusselt

number and a 5% to 12% increase in friction factor when compared to the DSS tubes. Notably, the tubes with d_0 = 2 mm displayed the highest Nusselt number and friction factor values. Furthermore, the PEC values were improved by 1.74%–5.14%, with the tubes featuring the largest PEC being those with d_0 = 1.5 mm.

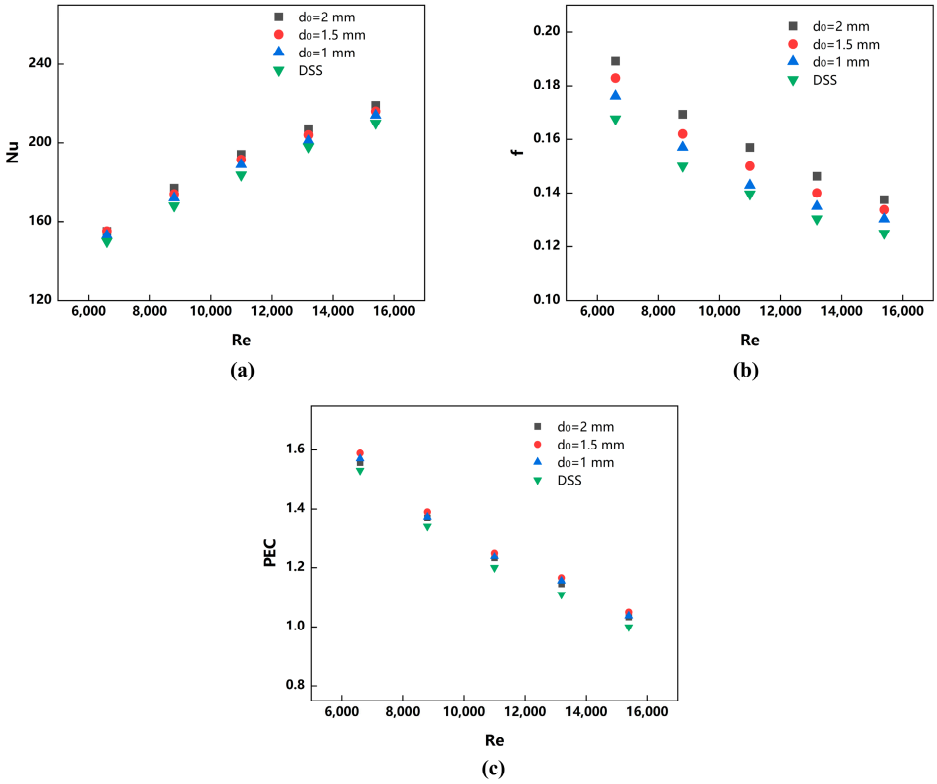


Figure 12. Variation in (**a**) Nusselt number, (**b**) friction factor, and (**c**) PEC, in terms of various d_0.

3.2.3. Effect of Key Shape

This study selected three distinct key shapes: circular, equilateral triangular, and square, as shown in Figure 13b from 1 to 3,while maintaining consistent parameters (pitch P = 10 mm, wire diameter e = 2 mm, and identical cross-sectional areas) for numerical simulation. Figure 13a,b illustrate these simulations, while Figure 13c–e demonstrate the relationships between Nu, f, PEC, and the Reynolds number.

The results presented in Figure 13 show the variations in the Nusselt number, friction factor, and PEC for the tubes using three different key shapes, as functions of Reynolds number. The findings indicate that the DSI with the square key shape enhances the Nusselt number the most significantly, followed by the circular key shape, while the triangular key shape demonstrates relatively lower performance. Moreover, the square and circular DSIs exhibit greater friction factors compared to the triangular DSI. The continuous curve surface of the circular key helps to minimize fluid separation and vortex formation, resulting in lower resistance; however, the square DSI's corner design promotes earlier fluid separation and larger vortex areas, consequently increasing resistance. This vortex also contributes to thinning of the boundary layer, enhancing the Nusselt number. Although triangular keys can also enhance heat transfer, their disturbance and boundary layer disruption effects are less pronounced than those of square keys. The sharper edges of the triangular key facilitate smoother fluid flow along the key's surface, reducing the degree of flow separation. The leading edge of the triangular key guides the fluid more smoothly, leading to less vortex formation and lower resistance. Compared to the triangular DSI, the square and circular DSI tubes exhibit friction factors that increase by 5.45% to 23.87% and 7.77% to

26.92%, respectively. The results in Figure 13e indicate that the square cross-section DSI tube exhibits the best comprehensive heat transfer performance, followed by the triangular cross-section DSI, with the circular cross-section DSI performing the least efficiently. Hence, selecting the square cross-section DSI as a research focus is practically significant.

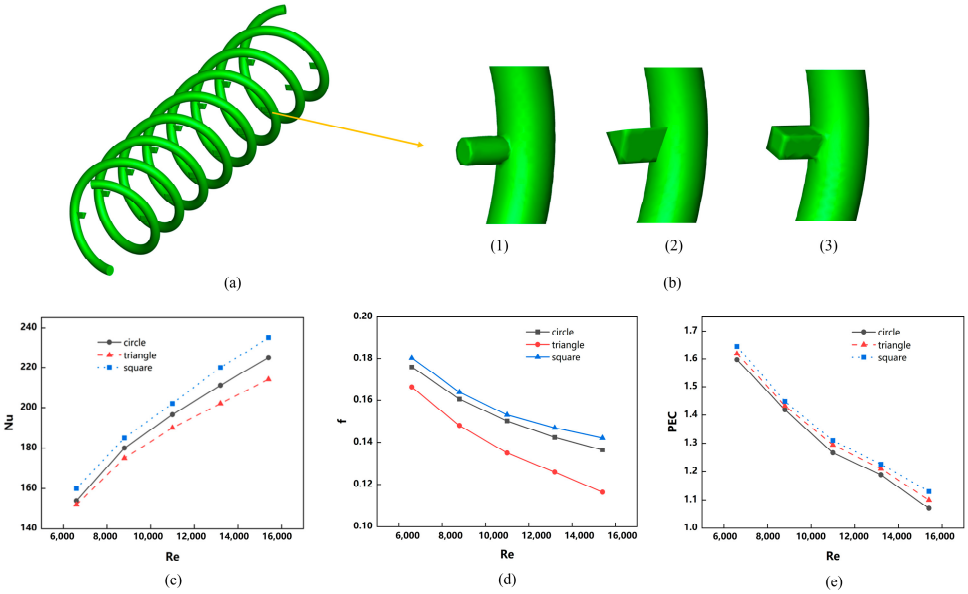


Figure 13. Schematic of heat exchange tubes with different DSI configurations. (**a**) 3D view of tube with tri-angular structure; (**b**) detailed view; (**c**) Nusselt number in terms of various pitches; (**d**) friction factor in terms of various pitches; (**e**) PEC in terms of various pitches.

4. Conclusions

This study presents a novel double-helical slotted insert inspired by DNA structures (DSI), and conducts a numerical investigation within a Reynolds number range of 6600–17,200. The conclusions of the research are as follows:

(1) The introduction of the DSI into smooth tubes significantly enhances heat transfer efficiency. The DSI promotes the formation of spiral fluid motion, effectively strengthening secondary flow effects, which is reflected in both the development of turbulence within the tube and the temperature distribution. However, the incorporation of the DSI also leads to increased pressure loss in the fluid flow.

(2) Under constant geometric parameters, a greater pitch results in a lower Nusselt number and friction factor for the heat exchange tube, with the PEC value being maximized at a pitch of 10 mm, at which pitch its PEC values are all above 1.

(3) Increased key length correlates with a higher Nusselt number and friction factor, with the DSI with a key length of 1.5 mm showing the highest PEC value. Similarly, the PEC value of the DSI with a key length of 2 mm is slightly lower than that with a length of 1 mm, yet both values surpass those of the DSS tube, demonstrating the advantages of the DSI in enhancing heat transfer.

(4) The shape of the keys within the DSI also significantly impacts heat transfer performance. The square cross-section DSI tube exhibits both higher Nusselt numbers and higher friction factors, ultimately resulting in the best PEC value.

Author Contributions: P.Z. carried out the formal analysis and contributed to the writing of the original draft; G.S. carried out the validation and contributed to the resources; R.L. carried out the investigation work; S.Z. (Sicong Zhou) carried out the validation and software-related work; B.H. carried out data curation and supervision; S.Z. (Shaofeng Zhang) carried out writing—review &

ed-iting and project administration. All authors have read and agreed to the published version of the manuscript.

Funding: This research received no external funding.

Data Availability Statement: The original contributions presented in this study are included in the article. Further inquiries can be directed to the corresponding author.

Conflicts of Interest: Author Guoxiu Sun was employed by the company Hebei Zetian Chemical Co., Ltd. The remaining authors declare that the research was conducted in the absence of any commercial or financial relationships that could be construed as a potential conflict of interest.

Nomenclature

Cp	specific heat capacity
D	inner tube diameter, mm
f	friction factor
f_0	friction factor in plain tube
f_i	friction factor in tube with internal inserts
h	convective heat transfer coefficient, $W{\cdot}m^{-2}\ K^{-1}$
L	tube length, mm
Nu	Nusselt number
N_i	Nusselt number in plain tube
N_0	Nusselt number in tube with internal inserts
P	pitch of DSI
p	static pressure, Pa
Re	Reynolds number
T	temperature, K
T_w	wall temperature
T_f	fluid temperature
u	velocity, m/s
u_i	velocity components, m/s
u_m	mean velocity, m/s

Greek Symbols

λ	thermal conductivity, $W{\cdot}m^{-2}\ K^{-1}$
λs	thermal conductivity of solid region., $W{\cdot}m^{-2}\ K^{-1}$
μ	kinematic viscosity, $kg{\cdot}s^{-1}{\cdot}m^{-1}$
ρ	density, kg/m^3

Abbreviations

DSI	DNA-inspired Slotted Insert
DSS	Double-Spiral Spring
PEC	performance evaluation criterion

References

1. Awais, M.; Bhuiyan, A.A. Heat transfer enhancement using different types of vortex generators (VGs): A review on experimental and numerical activities. *Therm. Sci. Eng. Prog.* **2018**, *5*, 524–545. [CrossRef]
2. Kanizawa, F.T.; Mogaji, T.S.; Ribatski, G. Evaluation of the heat transfer enhancement and pressure drop penalty during flow boiling inside tubes containing twisted tape insert. *Appl. Therm. Eng.* **2014**, *70*, 328–340. [CrossRef]
3. Sarmadian, A.; Moghaddam, H.A.; Asnaashari, A.; Joushani, H.A.N.; Moosavi, M.; Islam, M.S.; Saha, S.C.; Shafaee, M. Flow boiling heat transfer and pressure drop characteristics of Isobutane in horizontal channels with twisted tapes. *Int. J. Heat Mass. Transf.* **2020**, *162*, 120345. [CrossRef]

4. Fan, J.F.; Ding, W.K.; Zhang, J.F.; He, Y.L.; Tao, W.Q. A performance evaluation plot of enhanced heat transfer techniques oriented for energy-saving. *Int. J. Heat. Mass. Transf.* **2009**, *52*, 33–44. [CrossRef]
5. Kanizawa, F.T.; Mogaji, T.S.; Ribatski, G. A new model for flow boiling heat transfer coefficient inside horizontal tubes with twisted-tape inserts. *Int. J. Refrig.* **2016**, *61*, 55–68. [CrossRef]
6. Brough, D.; Ramos, J.; Delpech, B.; Jouhara, H. Development and validation of a TRNSYS type to simulate heat pipe heat exchangers in transient applications of waste heat recovery. *Int. J. Thermofluids* **2021**, *9*, 100056. [CrossRef]
7. Varun; Garg, M.O.; Nautiyal, H.; Khurana, S.; Shukla, M.K. Heat transfer augmentation using twisted tape inserts: A review. *Renew. Sustain. Energy Rev.* **2016**, *63*, 193–225. [CrossRef]
8. Yu, C.L.; Cui, Y.L.; Zhang, H.Q.; Gao, B.J.; Zeng, M.; Han, L. Comparative study on turbulent flow characteristics and heat transfer mechanism of a twisted oval tube with different twisted tapes. *Int. J. Therm. Sci.* **2022**, *174*, 107455. [CrossRef]
9. Yu, C.L.; Zhang, H.Q.; Zeng, M.; Wang, R.J.; Gao, B.J. Numerical study on turbulent heat transfer performance of a new compound parallel flow shell and tube heat exchanger with longitudinal vortex generator. *Appl. Therm. Eng.* **2020**, *164*, 114449. [CrossRef]
10. Webb, R.L. Performance evaluation criteria for use of enhanced heat transfer surfaces in heat exchanger design. *Int. J. Heat. Mass. Transf.* **1981**, *24*, 715–726. [CrossRef]
11. Khoshvaght-Aliabadi, M.; Sartipzadeh, O.; Alizadeh, A. An experimental study on vortex-generator insert with different arrangements of delta-winglets. *Energy* **2015**, *82*, 629–639. [CrossRef]
12. Rahgozar, S.; Maciel, Y.; Schlatter, P. Spatial resolution analysis of planar PIV measurements to characterise vortices in turbulent flows. *J. Turbul.* **2013**, *14*, 37–66. [CrossRef]
13. Yilmaz, I.H.; Mwesigye, A.; Göksu, T.T. Enhancing the overall thermal performance of a large aperture parabolic trough solar collector using wire coil inserts. *Sustain. Energy Technol. Assess.* **2020**, *39*, 100696. [CrossRef]
14. Tahir, S.; Mital, M. Numerical investigation of laminar nanofluid developing flow and heat transfer in a circular channel. *Appl. Therm. Eng.* **2012**, *39*, 8–14. [CrossRef]
15. Eren, H.; Celik, N.; Yildiz, S.; Durmus, A. Heat Transfer and Friction Factor of Coil-Springs Inserted in the Horizontal Concentric Tubes. *J. Heat. Transf-Trans. ASME* **2010**, *132*, 011801. [CrossRef]
16. Gunes, S.; Ozceyhan, V.; Buyukalaca, O. Heat transfer enhancement in a tube with equilateral triangle cross sectioned coiled wire inserts. *Exp. Therm. Fluid Sci.* **2010**, *34*, 684–691. [CrossRef]
17. Omidi, M.; Farhadi, M.; Darzi, A.A.R. Numerical study of heat transfer on using lobed cross sections in helical coil heat exchangers: Effect of physical and geometrical parameters. *Energy Conv. Manag.* **2018**, *176*, 236–245. [CrossRef]
18. Dbouk, T.; Habchi, C. On the mixing enhancement in concentrated non-colloidal neutrally buoyant suspensions of rigid particles using helical coiled and chaotic twisted pipes: A numerical investigation. *Chem. Eng. Process* **2019**, *141*, 107540. [CrossRef]
19. Mansour, M.; Khot, P.; Thévenin, D.; Nigam, K.D.P.; Zähringer, K. Optimal Reynolds number for liquid-liquid mixing in helical pipes. *Chem. Eng. Sci.* **2020**, *214*, 114522. [CrossRef]
20. Zhang, C.C.; Wang, D.B.; Zhu, Y.J.; Han, Y.; Wu, J.X.; Peng, X. Numerical study on heat transfer and flow characteristics of a tube fitted with double spiral spring. *Int. J. Therm. Sci.* **2015**, *94*, 18–27. [CrossRef]
21. Uniyal, V.; Joshi, S.K.; Kaushik, S.; Kanojia, N. (Eds.) CFD Investigation of transfer of the heat and turbulent flow in circular copper tube with perforated conical rings of aluminum material. In Proceedings of the 3rd International Conference on Futuristic Trends in Materials and Manufacturing (ICFTMM), Amsterdam, The Netherlans, 24–25 February 2021; Electrical Networks. Elsevier: Amsterdam, The Netherlands, 2021.
22. Nakhchi, M.E.; Esfahani, J.A. Numerical investigation of heat transfer enhancement inside heat exchanger tubes fitted with perforated hollow cylinders. *Int. J. Therm. Sci.* **2020**, *147*, 106153. [CrossRef]
23. Zeeshan, M.; Nath, S.; Bhanja, D. Determination of optimum winglet height of longitudinal vortex generators for the best thermo-hydraulic performance of compact heat exchangers. *J. Mech. Sci. Technol.* **2019**, *33*, 4529–4534. [CrossRef]
24. Li, J.Y.; Dang, C.B.; Hihara, E. Heat transfer enhancement in a parallel, finless heat exchanger using a longitudinal vortex generator, Part A: Numerical investigation. *Int. J. Heat Mass Transf.* **2019**, *128*, 87–97. [CrossRef]
25. Wang, Y.F.; Liu, P.; Shan, F.; Liu, Z.C.; Liu, W. Effect of longitudinal vortex generator on the heat transfer enhancement of a circular tube. *Appl. Therm. Eng.* **2019**, *148*, 1018–1028. [CrossRef]
26. Liang, Y.M.; Liu, P.; Zheng, N.B.; Shan, F.; Liu, Z.C.; Liu, W. Numerical investigation of heat transfer and flow characteristics of laminar flow in a tube with center-tapered wavy-tape insert. *Appl. Therm. Eng.* **2019**, *148*, 557–567. [CrossRef]
27. Zemaitis, A.; Miksys, J.; Gaidys, M.; Gecys, P.; Gedvilas, M. High-efficiency laser fabrication of drag reducing riblet surfaces on pre-heated Teflon. *Mater. Res. Express* **2019**, *6*, 065309. [CrossRef]
28. Khosravi, M.; Sadi, M.; Arabkoohsar, A.; Ebrahimi-Moghadam, A. Numerical Investigation of the Thermo-Hydraulic Characteristics for Annular Vortex Tube: A Comparison With Ranque-Hilsch Vortex Tube. *J. Energy Resour. Technol-Trans. ASME* **2020**, *142*, 10. [CrossRef]

29. Tanious, A.S.; Halawa, T. Potential of implementing DNA shape in heat transfer applications: A numerical study. *Therm. Sci. Eng. Prog.* **2023**, *44*, 25. [CrossRef]
30. Nasr, M.R.J.; Khalaj, A.H.; Mozaffari, S.H. Modeling of heat transfer enhancement by wire, coil inserts using artificial neural network analysis. *Appl. Therm. Eng.* **2010**, *30*, 143–151. [CrossRef]

Disclaimer/Publisher's Note: The statements, opinions and data contained in all publications are solely those of the individual author(s) and contributor(s) and not of MDPI and/or the editor(s). MDPI and/or the editor(s) disclaim responsibility for any injury to people or property resulting from any ideas, methods, instructions or products referred to in the content.